

Pairing and Superconductivity from weak to strong coupling in the Attractive Hubbard model

A. Toschi¹, P. Barone^{1,2}, M. Capone^{3,1,4}, and C. Castellani¹

¹ *INFM Center for Statistical Mechanics and Complexity SMC and Dipartimento di Fisica, Università di Roma “La Sapienza”, Piazzale Aldo Moro 2, I-00185 Roma, Italy*

² *Dipartimento di Fisica, Università Roma 3, Via della Vasca Navale 84, I-00146, Roma, Italy*

³ *Istituto dei Sistemi Complessi (ISC) del CNR, Via dei Taurini 19, 00185, Roma, Italy and*

⁴ *Enrico Fermi Center, Roma, Italy*

(Dated: June 15, 2021)

The finite-temperature phase diagram of the attractive Hubbard model is studied by means of the Dynamical Mean Field Theory. We first consider the normal phase of the model by explicitly frustrating the superconducting ordering. In this case we obtain a first-order pairing transition between a metallic phase and a paired phase formed by strongly coupled incoherent pairs. The transition line ends in a finite temperature critical point, but a crossover between two qualitatively different solutions still occurs at higher temperature. Comparing the superconducting and the normal phase solutions, we find that the superconducting instability always occurs before the pairing transition in the normal phase takes place, i.e., $T_c > T_{pairing}$. Nevertheless, the high-temperature phase diagram at $T > T_c$ is still characterized by a crossover from a metallic phase to a preformed pair phase. We characterize this crossover by computing different observables that can be used to identify the pseudogap region, like the spin susceptibility, the specific heat and the single-particle spectral function.

PACS numbers: 71.10.Fd, 71.10.-w, 74.25.-q

I. INTRODUCTION

The attractive Hubbard model represents an invaluable tool to understand properties of pairing and superconductivity in systems with attractive interactions. The simplifications introduced in this model allow a comprehensive study of the evolution from the weak-coupling regime, where superconductivity is due to BCS pairing in a Fermi liquid phase, and a strong coupling regime, in which the system is better described in terms of bosonic pairs, whose condensation gives rise to superconductivity (Bose Einstein (BE) superconductivity)¹. It has been convincingly shown that such an evolution is a smooth crossover and the highest critical temperature is achieved in the intermediate regime where none of the limiting approaches is rigorously valid^{1,2}. A realization of such a crossover scenario has been recently obtained through the development of experiments on the condensation of ultracold trapped fermionic atoms³. In these systems the strength of the attraction can be tuned by means of a tunable Fano-Feschbach resonance, and the whole crossover can be described⁴.

In the context of high-temperature superconductivity, the intermediate-strong coupling regime in which incoherent pairs are formed well above the critical temperature has been invoked as an interpretation of the pseudogap phase². Moreover, since the early days of the discovery of these materials, the evolution with the doping level of both the normal- and the superconducting-phase properties induced some authors^{5,6} to recognize the fingerprints of a crossover between a relatively standard BCS-like superconductivity in the overdoped materials and a strong-coupling superconductivity associated to

Bose-Einstein condensation (BE) in the underdoped materials. Indeed at optimal doping the zero-temperature coherence length is estimated to be around 10–20 Å^{7,8}, i.e., much smaller than for conventional superconductors but still large enough to exclude the formation of local pairs.^{9,10}

It is understood that the attractive Hubbard model has not to be taken as a microscopic model for the cuprates, since a realistic description of the copper-oxygen planes of these materials unavoidably requires a proper treatment of strong Coulomb repulsion. This simplified model represents instead an ideal framework where the evolution from weak to strong coupling can be studied by simply tuning the strength of the attraction. The main aim of the present work is to identify if, and to which extent, at least some aspects of the phenomenology of the cuprates can be interpreted simply in terms of a crossover from weak to strong coupling.

The main simplifications introduced by the attractive Hubbard model can be summarized as (i) Neglect of repulsion. Even if some attraction has to develop at low energy, the large short-range Coulomb repulsion implies that the interaction must become repulsive at high-energy in real systems. In some sense, an attractive Hubbard model picture can at most be applied to the low-energy quasiparticles. (ii) The model naturally presents s-wave superconductivity, as opposed to the d-wave symmetry observed in the cuprates (iii) Neglect of retardation effects. The Hubbard model describes instantaneous interactions, while every physical pairing is expected to present a typical energy scale.

The model is written as

$$\mathcal{H} = -t \sum_{\langle ij \rangle > \sigma} c_{i\sigma}^\dagger c_{j\sigma} - U \sum_i \left(n_{i\uparrow} - \frac{1}{2} \right) \left(n_{i\downarrow} - \frac{1}{2} \right) + \mu \sum_i (n_{i\uparrow} + n_{i\downarrow}) \quad (1)$$

where $c_{i\sigma}^\dagger$ ($c_{i\sigma}$) creates (destroys) an electron with spin σ on the site i and $n_{i\sigma} = c_{i\sigma}^\dagger c_{i\sigma}$ is the number operator; t is the hopping amplitude and U is the Hubbard on-site attraction (we take $U > 0$, with an explicit minus sign in the hamiltonian). Notice that, with this notations, the Hamiltonian is explicitly particle-hole symmetric for $\mu = 0$, which therefore corresponds to $n = 1$ (half-filling).

Despite its formal simplicity, this model can be solved exactly only in $d = 1$, while in larger dimensionality analytical calculations are typically limited to weak ($U \ll t$) or strong ($U \gg t$) coupling, where the BCS and the BE approaches are reliable approximations. It is anyway known that for $d \geq 1$, the ground state of (1) is superconducting for all values of U and all densities n , with the only exception of the one-dimensional half-filled case. At half-filling the model has an extra-symmetry and the superconducting and the charge-density-wave order parameters become degenerate.

A reliable description of the evolution of the physics as a function of U requires to treat the two limiting regimes on equal footing overcoming the drawbacks of perturbative expansions. Quantum Monte Carlo (QMC) simulations represent a valuable tool in this regard, and they have been applied to the two^{2,11,12,13,14} and three¹⁵ dimensional attractive Hubbard model. Even if the sign problem does not affect these simulations, finite size effects and memory requirements still partially limit the potentiality of this approach.

A different non perturbative approach is the Dynamical Mean-Field Theory (DMFT), that neglects the spatial correlations beyond the mean field level in order to fully retain the local quantum dynamics, and becomes exact in the limit of infinite dimensions¹⁶. Due to the local nature of the interaction in the attractive Hubbard model, we expect that the physics of local pairing is well described in DMFT. Moreover, this approach is not biased toward metallic or insulating states, and it is therefore particularly useful to analyze the BE-BCS crossover. On the other hand, the simplifications introduced by the DMFT are rigorously valid only in the infinite dimensionality limit, and even if the DMFT has obtained many successes for three dimensional systems, its relevance to lower dimensionality like $d = 2$ is much less established, and represents a fourth limitation of our study in light of a comparison with the physics of the cuprates. In particular, the role of dimensionality in determining the pseudogap properties of the attractive Hubbard model has been discussed in Refs.¹⁷.

The study of the attractive Hubbard model can greatly benefit of a mapping onto a repulsive model in a magnetic field. The mapping is realized in a bipartite lattice¹⁸ by

a 'staggered' particle-hole transformation on the down spins $c_{i\downarrow} \rightarrow (-1)^i c_{i\downarrow}^\dagger$. The attractive model with a finite density n transforms into a half-filled repulsive model with a finite magnetization $m = n - 1$. The chemical potential is transformed, accordingly, into a magnetic field $h = \mu$. In the $n = 1$ case (half-filling) the two models are therefore completely equivalent. We notice that the above mapping does not only hold for the normal phases, but extends to the broken symmetry solutions. The three components of the antiferromagnetic order parameter of the repulsive Hubbard model are in fact mapped onto a staggered charge-density-wave parameter (z component of the spin) and an s-wave superconducting order parameter ($x-y$ components). The above mapping is extremely useful, since it allows to exploit all the known results for the repulsive model and for the Mott-Hubbard transition to improve our understanding of the attractive model.

In recent works the DMFT has been used to study the normal phases of the attractive Hubbard model. In particular, a phase transition has been found both at finite¹⁹ and at zero temperature²⁰ between a metallic solution and an pairing phase of pairs. The insulating pairs phase is nothing but a realization of a superconductor without phase coherence, i.e., a collection of independent pairs. As it has been discussed in Ref.^{19,20}, this phase is the 'negative- U ' counterpart of the paramagnetic Mott insulator found for the repulsive Hubbard model. We notice that the insulating character of the pairing phase is a limitation of the DMFT approach, in which the residual kinetic energy of the preformed pairs is not described. The pairing transition has been first identified in Ref.¹⁹ by means of a finite temperature QMC solution of the DMFT. The $T = 0$ study of Ref.²⁰ has clarified that the pairing transition is always of first order except for the half-filled case, and that it takes place with a finite value of the quasiparticle weight $Z = (1 - \partial\Sigma(\omega)/\partial\omega)^{-1}$, associated to a finite spectral weight at the Fermi level. In the latter paper, it has also been shown that the pairing transition gives rise to phase separation.

For what concerns the onset of superconductivity, a DMFT calculation of the critical temperature T_c has been performed for the case of $n = 0.5$ in the same Ref.¹⁹. The T_c curve, extracted from the divergence of the pair-correlation function in the normal phase, displays a clear maximum at intermediate coupling and reproduces correctly both the BCS and the BE predictions in the asymptotic limits, remaining finite for all $U \neq 0$.

In this work we complement the analysis of Ref.²⁰, by extending our phase diagram to finite temperature, still using Exact Diagonalization (ED) to solve the impurity model associated with the DMFT of the Hubbard model²¹. We also compare the normal state solutions with the superconducting solutions which are stable at low temperatures. The use of ED allows us to reach arbitrarily small temperatures which are hardly accessible by means of QMC. Quite naturally, the extension of ED to finite temperature requires a more severe truncation of the Hilbert space. We have checked that all the thermo-

dynamical quantities we show are only weakly dependent on the truncation. The plan of the paper is the following: in Sec. II we briefly introduce the DMFT method and its generalization to the superconducting phase; In Sec. III we discuss the finite temperature phase diagram in the normal phase characterizing the low-temperature pairing transition; In Sec. IV we analyze the superconducting solutions; In Sec. V we compare different estimators of the pseudogap temperature in the high-temperature normal phase. Sec. VI contains our concluding remarks.

II. METHOD

The DMFT extends the concept of classical mean-field theories to quantum problems, by describing a lattice model in terms of an effective dynamical local theory. The latter can be represented through an impurity model subject to a self-consistency condition, which contains all the information about the original lattice structure through the non-interacting density of states (DOS)¹⁶. Starting from the Hubbard model (1), we obtain an attractive Anderson impurity model

$$\begin{aligned} \mathcal{H}_{AM} = & - \sum_{k,\sigma} V_k c_{k,\sigma}^\dagger c_{0,\sigma} + H.c. + \sum_{k,\sigma} \epsilon_k c_{k,\sigma}^\dagger c_{k,\sigma} \\ & - U \left(n_{0\uparrow} - \frac{1}{2} \right) \left(n_{0\downarrow} - \frac{1}{2} \right) + \mu n_0, \end{aligned} \quad (2)$$

The self-consistency is expressed by requiring the identity between the local self-energy of the lattice model and the impurity self-energy

$$\Sigma(i\omega_n) = \mathcal{G}^0(i\omega_n)^{-1} - G(i\omega_n)^{-1}, \quad (3)$$

where $G(i\omega_n)$ is the local Green's function of (2), and $\mathcal{G}^0(i\omega_n)^{-1}$ is the dynamical Weiss field, related to the parameters in (2) by

$$\mathcal{G}^0(i\omega_n)^{-1} = i\omega_n + \mu - \sum_k \frac{V_k^2}{i\omega_n - \epsilon_k}. \quad (4)$$

By expressing the local component of the Green's function in terms of the lattice Green's function, namely $G(r=0, i\omega_n) = \sum_k G(k, i\omega_n)$, Eq. (3) implies

$$\mathcal{G}^0(i\omega_n)^{-1} = \left(\int d\epsilon \frac{D(\epsilon)}{i\omega_n + \mu - \epsilon - \Sigma(i\omega_n)} \right)^{-1} + \Sigma(i\omega_n), \quad (5)$$

where $D(\epsilon)$ is the non interacting density of states of the original lattice. We consider the infinite-coordination Bethe lattice, with semicircular DOS of half-bandwidth D (i.e., $D(\epsilon) = (2/\pi D^2) \sqrt{D^2 - \epsilon^2}$), for which Eq. (5) is greatly simplified and becomes

$$\mathcal{G}^0(i\omega_n)^{-1} = i\omega_n + \mu - \frac{D^2}{4} G(i\omega_n). \quad (6)$$

In this work we also consider solutions with explicit s-wave superconducting order, by allowing for local anomalous Green's functions $F(\tau) = -\langle T_\tau c_{0\uparrow}(\tau) c_{0\downarrow} \rangle$. The

whole DMFT formalism can then be recast in Nambu-Gorkov spinorial representation¹⁶, and Eqs. (3) and (5) must be read as matrix identities in the Nambu space. As far as the impurity model is concerned, we need to describe an Anderson impurity model with a superconducting bath or, equivalently, with an anomalous hybridization in which Cooper pairs are created and destroyed in the electronic bath, i.e., a term $\sum_k V_k^s (c_{k\uparrow} c_{k\downarrow} + H.c.)$ is added to (2).

The heaviest step of the DMFT approach is to compute $G(i\omega_n)$ for the Anderson model (2). This solution requires either a numerical approach or some approximation. Here we use Exact Diagonalization. Namely, we discretize the Anderson model, by truncating the sums over k in Eqs. (2) and (4) to a finite number of levels N_s . It has been shown that extremely small values of N_s provide really good results for thermodynamic properties and reliable results for spectral functions. In this work we use the ED approach at finite temperature, where it is not possible to use the Lanczos algorithm, which allows to find the groundstate of extremely large matrices. To obtain the full spectrum of the Hamiltonian, needed to compute the finite-temperature properties, we are forced to a rather small value of N_s , up to 6. All the results presented here are for $N_s = 6$, and we always checked that changing N_s from 5 to 6 does not affect the relevant observables we discuss in the present work, except for the real-frequency spectral properties.

III. THE PAIRING TRANSITION

In this section we limit our analysis to normal phase paramagnetic solutions in which no superconducting ordering is allowed. Even if the s-wave superconducting solution is expected to be the stable one at low temperatures, our normal state solutions are representative of the normal phase above the critical temperature. The region in which the normal state is stable may of course be enlarged by frustrating superconductivity through, e.g., a magnetic field. Moreover, the nature of the normal phase gives important indications on the nature of the pairing in the different regions of the phase diagram. As mentioned above, it has been shown that the normal phase of the attractive Hubbard model is characterized by a "pairing" transition between a Fermi-liquid phase and a phase in which the electrons are paired, but without any phase coherence among the pairs.

The pairing transition has been first discussed at finite temperature in Ref.¹⁹, and a complete characterization at $T = 0$ has been given in Ref.²⁰. In this paper we complete the finite temperature study of the transition and connect it to the zero-temperature phase diagram, finally drawing a complete phase diagram in the attraction-temperature plane for a density $n = 0.75$, taken as representative of a generic density (except for the peculiar particle-hole symmetric $n = 1$ case). This situation would correspond to a repulsive model at half-filling in an external mag-

netic field tuned to give a finite magnetization $m = 0.25$. The $T = 0$ DMFT solution of the attractive Hubbard model is characterized by the existence of two distinct solutions, a metallic one with a finite spectral weight at the Fermi level and an insulating solution formed by pairs, with no weight at the Fermi level. The previous study has also clarified that the quasiparticle weight $Z = (1 - \partial\Sigma(\omega)/\partial\omega)^{-1}$, which may be used as a sort of order parameter for the Mott transition at half-filling, loses this role for the doped attractive Hubbard model, being it finite both in the metallic and pairing phases. At $T = 0$, the metallic solution exists only for $U < U_{c2}$, and the insulating one for $U > U_{c1}$, with $U_{c1} < U_{c2}$. In other words, a coexistence region is present where both solutions exist, and where the actual ground state is determined minimizing the internal energy. The clear-

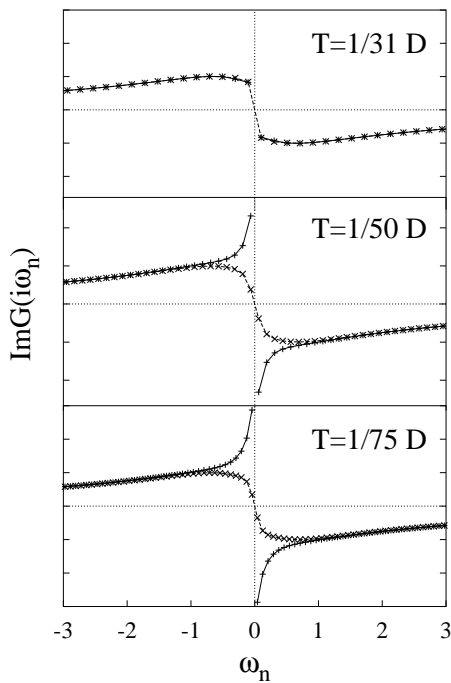


FIG. 1: Evolution of the imaginary part of the Green's function as a function of temperature for $U/D = 2.4$. In each panel are shown the metallic (+) and insulating (x) solutions. (the chosen value of the attraction lies in the coexistence region).

cut $T = 0$ characterization of the two solutions based by the low-energy spectral weight is lost at finite temperature, where both solution have finite weight at the Fermi level. Nonetheless, two families of solutions can still be defined, each family being obtained by continuous evolution of the different $T = 0$ phases. The two solutions are still clearly identified at relatively low temperatures, further increasing the temperature, the differences between the two solutions is gradually washed out, as shown in Fig. 1, where we plot the tempera-

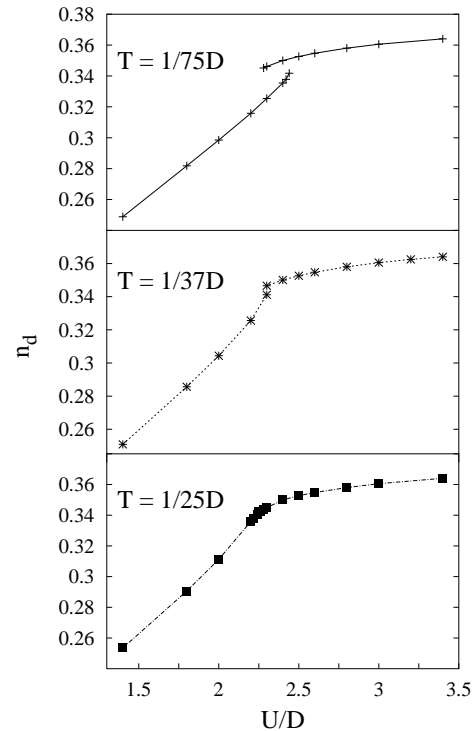


FIG. 2: Average double occupancy as a function of the attraction strength for different temperatures. The first order transition at low temperatures becomes a continuous evolution at high temperatures, where there is no more distinction between metallic and pairing solutions.

ture evolution of the imaginary part of the Green's function in imaginary frequency for $U = 2.4D$, which lies in the $T = 0$ coexistence region. While at $T = 1/75D$ and $T = 1/50D$ the difference in the two solutions is still clear, at $T = 1/31D$, the two solutions become basically indistinguishable. This result suggests that, as intuitively expected, the temperature reduces the difference between the solutions and consequently, the size of the coexistence region, which is expected to close at some finite temperature critical point (the attractive counterpart of the endpoint of the line of metal-insulator transitions in the repulsive model²²). A similar information is carried by the analysis of the average value of double occupancy $n_d = \langle n_\uparrow n_\downarrow \rangle$. This quantity naturally discriminates between an pairing phase with a large value of n_d and a metal with a smaller value. As shown in Fig. 2, at low temperature we have two solutions with a different value of n_d in the coexistence region, and a jump in this quantity at the transition. Upon increasing the temperature, the two solutions tend to join smoothly one onto the other, signaling again the closure of the coexistence region, which is substituted by a crossover region. Analogous behavior is displayed by the quasiparticle weight Z .

Repeating the same analysis for a wide range of coupling constants and temperatures, we are able to construct a finite-temperature phase diagram for the pairing transition, shown in Fig. 3. For temperatures smaller than a critical temperature $T_{pairing}$, we compute the finite temperature extensions of U_{c1} and U_{c2} , which mark the boundary of the coexistence region. The two lines (depicted as dashed lines in Fig. 3) converge into a finite temperature critical point at $U = U_{pairing} \simeq 2.3D$ and $T = T_{pairing} \simeq 0.03D$. Despite the closure of the coexistence region, a qualitative difference between weak coupling and strong coupling solutions can still be identified for $T > T_{pairing}$, determining a crossover region in which the character of the solution smoothly evolves from one limit to the other as the attraction is tuned. At this stage, the crossover region is “negatively” defined as the range in which the Green’s function does not resemble any of the two low temperature phases. The crossover lines are estimated as the points in which it becomes impossible to infer from the Matsubara frequency Green’s function whether the low-energy behavior is metallic or insulating. It has been shown for the repulsive Hubbard model that this kind of crossover is accompanied by a qualitative difference in transport properties. In the region on the left of the crossover, the conduction is metallic and the resistivity increases with temperature. In the intermediate crossover region the system behaves like a semiconductor with a resistivity which decreases upon heating, and finally in the phase on the right of the crossover region the system behaves like a heated insulator¹⁶.

Coming from the left, the first crossover occurs when $G(i\omega_n)$ has no longer a clear metallic behavior with a finite value at zero frequency, while the second crossover line delimits the region in which the gap of the paired solution is closed by thermal excitations. We will come back later to the crossover region and compare the above defined lines with physically sensible estimators of the pseudogap temperature, like the specific heat and the spin susceptibility.

Turning to the coexistence region, we can also ask ourselves which is the stable phase. This requires a comparison between the Gibbs free energies of the two phases. At half-filling, where the attractive and the repulsive model are equivalent, it has been shown that at $T = 0$ the metallic solution is stable in the whole coexistence region²³. At finite temperature it has been shown numerically that the insulator becomes stable in a large portion of the coexistence region due to its large entropy¹⁶. The transition is therefore of first order for all temperature below the critical temperature, except for the two second-order endpoints at $T = 0$ and $T = T_{pairing}$. For densities out of half-filling it has been shown in Ref. 20 that the transition is of first order already at $T = 0$ and it is accompanied by a small phase separation region. For $n = 0.75$, the $T = 0$ first-order transition occurs quite close to U_{c2} .

Analogously to the half-filling case, the finite temperature almost immediately favors the pairing phase. Indeed, computing the free energy following, e.g., Ref.²⁴,

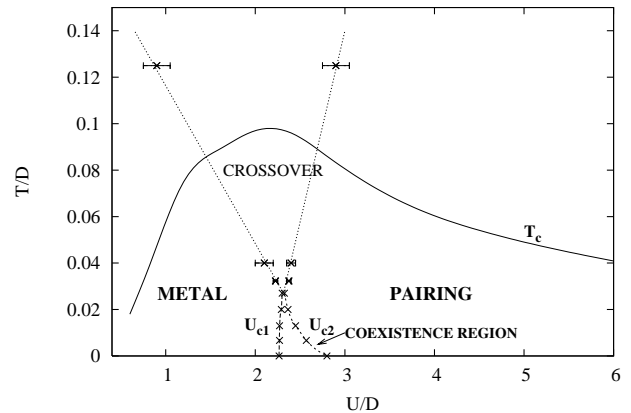


FIG. 3: Phase diagram in the U - T plane. At low temperature two critical lines $U_{c1}(T)$ and $U_{c2}(T)$ individuate the coexistence region. The two lines converge in a finite temperature critical point. At higher temperatures we can still define two crossover lines. The superconducting critical temperature is also drawn as a solid line (cfr. Fig. 4).

we find the pairing phase stable for almost every point in the coexistence region. We had to use an extremely dense mesh of points in the U direction to identify a small section where the metallic phase is stable at finite temperature. Therefore the finite temperature first-order transition occurs extremely close to the U_{c1} line for finite temperature and rapidly moves closer to U_{c2} only at really small temperatures.

IV. THE SUPERCONDUCTING PHASE

The above stability analysis has been restricted to normal phase solutions. Indeed the superconducting solution is expected to be the stable one at $T = 0$ for all densities and values of the interaction U . The critical temperature T_c is obtained directly as the highest temperature for which a non-vanishing anomalous Green’s function $F(\omega)$ exists.

The DMFT critical temperature T_c for $n = 0.75$ as a function of U is reported in Fig. 4 (full dots) and it qualitatively reproduces the limiting behavior, with an exponential BCS-like behavior for small U ’s and a $1/U$ decrease at large U according to the expression for the BE condensation temperature hard-core boson system²⁵. As a result, T_c assumes its maximum value of about $0.1D$ for an intermediate coupling strength $U_{max} \simeq 2.1D$. Interestingly, the maximum T_c occurs almost exactly at the coupling for which the pairing transition in the normal phase would take place in the absence of superconductivity.

It might be noticed however that, while the BE result (open triangles in Fig. 4) basically falls on top of the DMFT results, the BCS formula (open circles) only qualitatively follows the full solution. This “asymmetry”

in recovering the BCS behavior arises from the partial screening of the bare attraction due to second order polarization terms²⁶. Because of these corrections the attraction is renormalized as $U_{eff} \simeq U - AU^2/t$, so that $\frac{1}{U_{eff}} \simeq \frac{1}{U}(1 + AU/t) = 1/U + A/t$. When this correction is plugged in the BCS formula for T_c , it results in a correction to the prefactor. If we simply extract the rescaling factor for a given small value of U ($T_c/T_c^{BCS} \simeq 0.32$) and we simply scale the whole weak-coupling curve by this factor, we obtain the points marked with asterisks, whose agreement with the DMFT results does not require further comments. It is interesting, instead, to compare the DMFT estimations for T_c with the QMC results: despite the presence of many factors (such as the exact shape of the D.O.S. of the model or the finite dimension effects) which are capable to introduce relevant variations in the values of T_c , some general similarities appear clearly. Indeed, while simple rescaling the data in terms of the half-bandwidth D , both T_c and U_{max} estimations with the two^{12,13} and three¹⁵ dimensional QMC are lower than the DMFT evaluation (i.e., $T_c \sim 0.04D$, $U_{max} \sim 0.7D$ for the $d = 2$ case, and $T_c \sim 0.05D$, $U_{max} \sim 1.3D$ in $d = 3$, even if for a lower density of $n = 0.5$), one can observe, quite surprisingly, that the ratio between T_c and U_{max} is around $0.04 \div 0.05$ in both the DMFT and the two QMC cases.

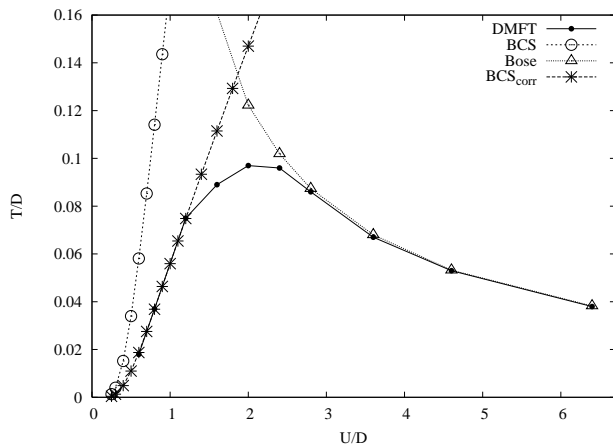


FIG. 4: Critical temperature as a function of U at $n = 0.75$: the DMFT data (black circle) are compared with the BCS -both the bare (empty circles) and the rescaled one (stars)- and the BE mean field predictions (empty triangles) for a hard-core boson systems (see Refs. 1,25).

Coming back to our DMFT results, the simplest and most important observation is that the critical temperature is always higher than the critical temperature for the pairing transition. For example in our $n = 0.75$ case, T_c^{max} is about $0.1D$, against a $T_{pairing}$ of $0.03D$. As a result, the whole phase transition is hidden by superconductivity, which remains as the only real instability of the system (cfr. Fig. 3). Nevertheless, the crossover lines at higher temperature survive the onset of superconductiv-

ity. Therefore the normal phase we reach for $T > T_c$ is really different according to the regime of coupling we are in. For weak-coupling, the normal phase is substantially a regular Fermi-liquid and superconductivity occurs as the standard BCS instability. In the strong-coupling regime, the normal phase is instead a more correlated phase which presents a pseudogap in the spectrum. At intermediate coupling, where the superconducting critical temperature reaches its maximum, the normal phase is in a crossover region between the two limiting behaviors.

V. THE PSEUDOGAP PHASE: SPIN SUSCEPTIBILITY, SPECIFIC HEAT AND SPECTRAL FUNCTIONS

Even if the onset of superconductivity completely hides the pairing transition, the fingerprints of the low-temperature normal phase are still visible in the high-temperature phase diagram, in which a crossover from a metallic phase to a gapped phase is still present. It is tempting to associate the region in which the system behaves as a collection of incoherent pairs to the pseudogap regime of the cuprates. It is important to underline that, in this framework, the definition of the pseudogap phase is somewhat tricky, and it implies a certain degree of arbitrariness. In this section we come back to this region and compute various observable whose anomalies have been used to identify the pseudogap phase and compare the related estimates of the pseudogap temperature T^* .

Our first estimate is based on the evaluation of the uniform spin susceptibility χ_s as a function of temperature for different attraction strengths. The opening of a gap in the spin excitation spectrum, not associated with any long-range order, represented in fact one of the first indications of existence of the pseudogap phase in high-temperature superconductors. The DMFT calculation of χ_s can be performed by evaluating the derivative of the magnetization m with respect to a uniform magnetic field in the limit of vanishing h . In terms of the local Green functions

$$\chi_s = \lim_{h \rightarrow 0} \frac{1}{2} T \frac{\sum_{\omega_n} [G_{\uparrow}(i\omega_n) - G_{\downarrow}(i\omega_n)]}{h}. \quad (7)$$

This calculations has been performed by varying the temperature in a wide range ($0 < T < 2D$) for four different values of the pairing interaction ($U/D = 0.8, 1.8, 2.4$ and 3.6) and represent an extension of the results reported in Ref. [19]. The results of our calculation are summarized in Fig. 5.

In the weak-coupling side ($U = 0.8D$) we find a conventional metallic behavior of χ_s , which increases monotonically with decreasing temperature. The interaction reduces the zero-temperature extrapolated value with respect to the non-interacting result $\chi_s = \rho(0)$. On the opposite side of the phase diagram, in the strong-coupling regime ($U = 3.6D$) the standard high-temperature be-

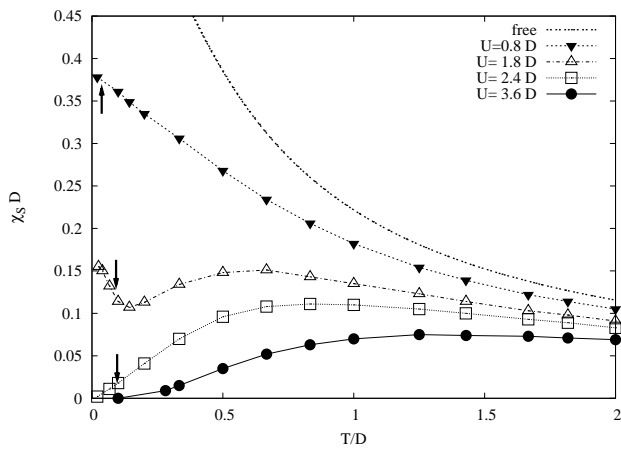


FIG. 5: Spin susceptibility in the normal phase as a function of temperature for $U/D = 0.0, 0.8, 1.8, 2.4, 3.6$. These values of U are representative of all the interesting region of the phase diagram in Fig. 3, moving from the metallic to the paired side. The values of the superconducting critical temperature are marked by small black arrows.

havior of χ_s extends only down to a certain temperature T_M^* , where a maximum of χ_s is reached. When the temperature is further reduced χ_s starts to decrease, exponentially approaching zero in the $T = 0$ limit, signaling the opening of a gap in the spin-excitation spectrum. A qualitatively similar behavior is found also in the intermediate-coupling regime, at least as long as the value of U stays larger than $U_{pairing}$ (e.g., $U = 2.4D$), or, in other words, as long as the left line defining the crossover region in Fig. 3 is not crossed. The behavior of χ_s becomes richer for $U = 1.8D < U_{pairing}$. At high temperatures χ_s closely resembles the insulating case, displaying a clear maximum at a temperature T_M^* . By approaching $T = 0$, χ_s no longer vanishes, but it rises at small temperatures displaying a minimum for a temperature lower than T_M^* : a metallic behavior is therefore recovered, associated to the narrow resonance at the Fermi level¹⁹. Such a behavior naturally defines a different temperature scale T_m^* , which is associated to the minimum of χ_s and represents the lower border of the pairing zone, or in a sense, of the “pseudogap” region. Conversely, this low-temperature behavior has not been observed to our knowledge in finite-dimensional QMC simulation^{2,11,12,13,14,15}. In practice, the system displays a pseudogap behavior in the region between T_m^* and T_M^* , whose boundary, labeled as T_s^* , is represented in Fig. 8.

We finally mention that the temperature T_M^* for which χ_s is maximum scales with U . This finding is in a qualitative agreement with a QMC simulation^{12,15}, where the $T_M^*(U)$ is taken as a definition of the temperature below which the pseudogap appears. From a more quantitative point of view, as happens for T_c and U_{max} , the values of $T_M^*(U)$ of the QMC simulations are lower than our DMFT results (i.e., $T_M^*(U_{max}) \sim 0.15D$ when $d = 2$

and $\sim 0.45D$ for $d = 3$, against the DMFT estimate of $\sim 0.7D$). However, also in this case the ratio between $T_M^*(U_{max})$ and U_{max} has a more universal value around $0.2 \div 0.3$.

Another relevant quantity is the specific heat $C_V = \partial E / \partial T = -T \partial^2 F / \partial T^2$, that we obtain by differentiating a fit to the DMFT internal energy $E(T)$ for the same attraction strengths and report in Fig. 6. Also for this quantity the weak coupling case ($U/D = 0.8$) behaves as a regular metal, with a linear behavior at small temperatures ($C_V = \gamma T$, with $\gamma \propto 1/m^*$, m^* being the effective mass). followed by a smooth decrease when the temperature exceeds the typical electronic energy scale. The same qualitative result is found for the noninteracting system, where the low- T slope is smaller since the interacting system has a larger effective mass. In the opposite strong coupling limit we observe the typical activated behavior of gapped systems for small temperatures, with an exponential dependence of $C_V(T)$ which extends up to a temperature T_{hM}^* large enough to wipe out the effect of the gap. It is therefore natural to associate such a temperature to the closure of the pseudogap.

In the most interesting $U = 1.8D$ case, two features are clearly present in the $C_V(T)$ curve. The first, low-temperature feature is the evolution of the small- U metallic feature, which acquires a larger slope as U/D is increased due to the enhancement of the effective mass, and shrinks as a consequence of the reduced coherence temperature of the metal. The second feature is instead the evolution of the large- U insulating one, and would show an activated behavior partially hidden by the low- T metallic peak. Thus, the system behaves like a metal in the small temperature range, while it has a pseudogap for intermediate temperature. We estimate the lower boundary of the pseudogap region in this intermediate coupling regime through the maximum of the low-temperature feature, which is controlled by the effective coherence scale of the metal. The upper bound is naturally defined as the temperature in which the activated behavior disappears. As a result, the specific heat analysis determines a pseudogap region with a very similar shape than the one determined through the spin susceptibility, with a re-entrance of metallic behavior in the intermediate coupling regime at low temperatures.

An inspection to the spectral function can strengthen our insight on the pseudogap phase. In principle the ED algorithm allows to directly compute finite frequency spectral functions $\rho(\omega) = -1/\pi \text{Im} G(\omega)$, avoiding the problems and ambiguities intrinsic with analytic continuation techniques. Unfortunately, the discretization of the Hilbert space which allows for an ED solution results in “spiky” local spectral functions formed by a collection of δ -functions. In this light, we find it useful to compute $\rho(\omega)$ by analytically continuing Eq.(3), analytically computing the local retarded Green function $G_{loc}(\omega) = -1/\pi \int d\epsilon D(\epsilon)(\omega - \epsilon + \mu - \Sigma_{ret}(\omega))^{-1}$. This procedure provides more “realistic” descriptions of both the non-interacting DOS and of the strong-coupling pair-

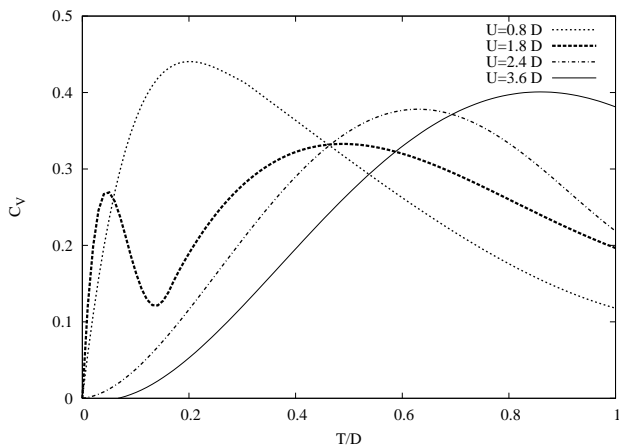


FIG. 6: Specific heat as a function of temperature for $U/D = 0.8, 1.8, 2.4, 3.6$. All the C_V lines are obtained by differentiating the the internal energy $E_{int}(T)$. The expression of $E_{int}(T)$ is computed directly by fitting the DMFT data.

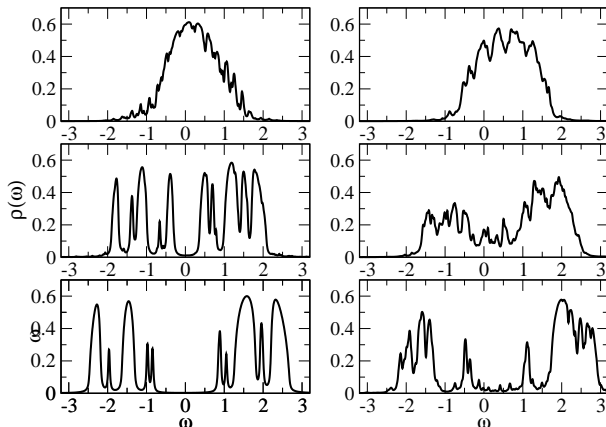


FIG. 7: Here are plotted the density of states $\rho(\omega)$ for three different values of the interaction: $U = 0.8D, 2.4D$ and 3.6 (from the upper to the lower row) both at the low-temperature ($T = 0.1D$, left panels) and at the high-temperature ($T = 1D$, right panels).

ing phase. However, even though the spectral functions are smoothed by this procedure, we can only extract informations about the gross features of the spectra as, e.g., the amplitude of the gap $\Delta(T)$. Keeping these limitations in mind, some results for $\rho(\omega)$ are plotted in Fig. 7: for the weak- ($U = 0.8D$), the intermediate- ($U = 2.4D$) and strong-coupling ($U = 3.6D$) case a low and high-temperature set of data are shown. Apart from the obvious appearing and enlarging of a gap in $\rho(\omega)$ with increasing U , which is evident in the low-temperature data, it should be noticed that both in the intermediate and the strong-coupling regime there is apparently no tendency to a ‘closure’ of such a gap when the temperature is raised. Indeed, as it is shown in the sec-

ond and the third row of Fig. 7, the gap starts to fill at some temperature ($T \sim 0.45D$ for $U = 2.4D$ and $T \sim 1.5 \div 2.0D$ for $U = 3.6D$), but for these values of U much of the spectral weight remains in the high-energy Hubbard bands, and the gapped structure does not completely vanish up to the highest temperature reached in our calculation ($T \simeq 2D$). On the other hand, QMC results in $d = 2^{13}$ obtained through maximum entropy show a closure of the gap in $\rho(\omega)$ at a temperature lower than our threshold. Further investigation is needed to understand whether the discrepancy is due to a different behavior between $d = 2$ and the infinite dimensionality limit, or it is determined by the technical difficulties involved in the calculation of real frequency spectra in both approaches. The persistence of the gap structure at high temperature that we find in DMFT is also obtained within a perturbative analysis of superconducting fluctuations at strong coupling in $d = 2^{27}$.

In Fig. 8 we compare our estimates of the pseudogap temperature obtained through different physical quantities. We draw the borders of the pseudogap region as determined from the spin susceptibility ($T_s^*(U)$) and the specific-heat behavior ($T_h^*(U)$ and the value of the superconducting gap Δ_0 at zero temperature: The upper borders of the spin and the specific-heat ‘‘pseudogap’’ region scale roughly with U , as Δ_0 does, so that both $T_h^*(U)$ and $T_s^*(U)$ are proportional to Δ_0 , as the experimentally determined pseudogap. At low temperature, the pseudogap region boundary as extracted from thermodynamic response functions displays a clear re-entrance, which can be associated with the onset of the low-temperature quasi-particle peak. We also notice that the low-temperature curve qualitatively follows the behavior of the $U_{c2}(T)$ line. As mentioned above, the slope of $U_{c2}(T)$ is easily interpreted in terms of entropy balance between the two phases, which favors the preformed pairs phase.

Our phase diagram also represents a warning regarding attempts to extrapolate the low-temperature behavior from the high-temperature data in order to compare with finite-dimensional QMC calculations. If one, as, e.g., in Ref. 15, extrapolated the high-temperature behavior down to $T = 0$ in order to estimate the metal-insulator point, would have obtained an estimate of U^* significantly lower than the real U_{c2} . This finding emphasize how the high-temperature properties of the attractive Hubbard model are only weakly dependent on dimensionality, as indicated by the similarity between DMFT and finite-dimension QMC, while the low-temperature behavior may well be dependent on the dimensionality, as well as on the details of the bandstructure of the underlying lattice.

VI. CONCLUSIONS

In this paper we have investigated the finite temperature aspects of pairing and superconductivity in the at-

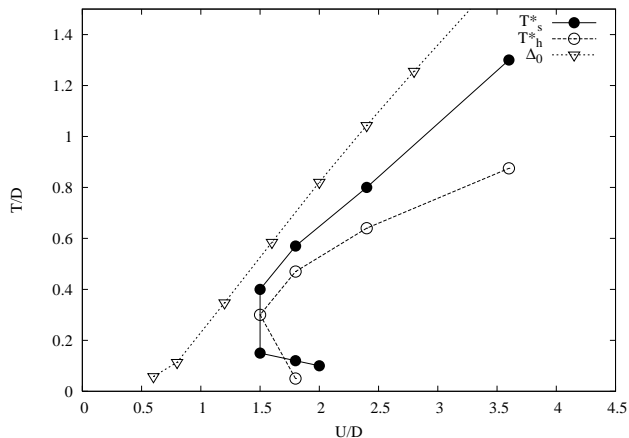


FIG. 8: Different estimates of the pseudogap temperature. The filled circles indicates $T_s^*(U)$, i.e., the temperatures of both the maxima and the minima of $\chi_s(T)$, while the empty circle marked $T_h(U)$ that is the temperature associated with the maxima and the minima of $C_V(T)$. The regions on the left of these two lines can be interpreted as the zone of “pseudogap” behavior for the spin and the specific heat respectively. These lines are then compared with the behavior of the anomalous part of the self-energy at zero temperature (Δ_0 , empty triangles).

tractive Hubbard model by means of DMFT, considering both normal and superconducting solutions.

In the normal phase we have identified two families of solutions, a Fermi-liquid metallic phase and a preformed-pair phase with insulating character. The latter phase is formed by local pairs without phase coherence. A finite region of the coupling-temperature phase diagram is characterized by the simultaneous presence of both solutions. In the low temperature regime a first-order transition occurs within this region when the free energies of the two solutions cross, and the region closes at a certain temperature ($T_{pairing} = 0.03D$) in a critical point. Interestingly, some trace of the two solutions survives even for temperature larger than the critical temperature, and two crossover lines can be defined separating a normal metal, a sort of semiconductor in which the gap is closed by temperature, and the preformed-pair phase with a well defined gap.

When superconductivity is allowed, the superconducting solution is stable for all values of the attraction and the critical temperature is always larger than the pairing transition temperature in the normal phase. In the superconducting state, we find an evolution from a weak-coupling BCS-like behavior, with exponentially small T_c from a normal metal to the superconductor, and a strong-coupling regime in which superconductivity is associated to the onset of the phase-coherence among the preformed pairs that occurs at $T_c \propto t^2/U$. The highest T_c is obtained in the intermediate region between this two limiting cases, namely for $U \simeq 2.1D$, which is extremely

close to the zero-temperature critical point of the normal phase.

The presence of the pairing transition affects the normal phase above T_c also when superconductivity establishes. In particular, one could be tempted to identify the phase of preformed pairs obtained at strong coupling with the pseudogap behavior observed in cuprates. In order to test the adequacy of such an identification, we computed different observables, whose anomalies can identify the appearance of the pseudogap, like the spin susceptibility, the specific heat and the single particle spectral functions. In the intermediate region of coupling, where the pairing transition occurs and the superconducting critical temperature reaches its maximum, the pseudogap region presents a re-entrance at low temperatures associated with a small coherent peak in the spectral function. At temperatures smaller than this coherence temperature the system behaves like a normal metal with renormalized effective mass. On the other hand, the high-temperature boundary of the pseudogap region scales with U regardless the criterion we use to estimate it. The estimate of the pseudogap temperature from specific heat and spin susceptibility both scale with the zero-temperature gap, as in the cuprates.

The most striking difference between our pseudogap phase-diagram and the experiments in the cuprates is that the pseudogap phase in the attractive Hubbard model is much larger than the experimental one, as it is measured by the large value of $T_{s,h}^*/T_c \simeq 5$ at the optimal value of the attraction. The experimental T^* around optimal doping is instead very close to T_c , and, according to some authors, the pseudogap line tends to zero at optimal doping. Moreover, the pseudogap temperature observed in the cuprates is definitely much smaller than the one found within our DMFT of the attractive Hubbard model. This inadequacy of the attractive Hubbard model in describing some features of the pseudogap phase descend from the above mentioned strong simplifications of the model (neglect of retardation effects, Coulomb repulsion and d-wave symmetry of the gap) and of our DMFT treatment which is exact only in the infinite dimensionality limit. One could be tempted in maintaining an attractive Hubbard model description for the quasiparticles alone, but it is important to point out that this interpretation can not be pushed too far. As an example, it is clear that such a description would fail for temperatures larger than the quasiparticle renormalized bandwidth.

A better description of the pseudogap phase would require models in which both an attraction and a repulsion are present. This is for instance the case of the models introduced in Refs. 28,29, where the superconducting phenomenon only involves heavy quasiparticles which experience an unscreened attraction and a richer behavior of the pseudogap (which in this case closes around optimal doping) is found.

VII. ACKNOWLEDGMENTS

and G. Sangiovanni.

This work is also supported by MIUR Cofin 2003. We acknowledge useful discussions with S. Ciuchi, M. Grilli,

-
- ¹ R. Micnas, J. Ranninger, and S. Robaskiewicz, *Rev. Mod. Phys.* **62**, 113 (1990).
- ² See, e.g., M. Randeria, J. Duan, and L. Shieh, *Phys. Rev. Lett.* **981**, (1989); M. Randeria, N. Trivedi, A. Moreo, and R.T. Scalettar, *Phys. Rev. Lett.* **69**, 2001, (1992);
- ³ M. Greiner, C.A. Regal, and D.S. Jin, *Nature* **426**, 537 (2003); S. Jochim, M. Bartelstein, A. Altmeyer, G. Hendl, S. Riedl, C. Chin, J. Hecker Denschlag, and R. Grimm, *Science* **302**, 2101 (2003).
- ⁴ A. Perali, P. Pieri, L. Pisani, and G.C. Strinati, *Phys. Rev. Lett.* **92**, 2204004 (2004).
- ⁵ C. A. R. Sá de Melo *et al.*, *Phys. Rev. Lett.* **71**, 3202 (1993); R. Haussmann, *Z. Phys. B* **91**, 291 (1993); V.J. Emery and S.A. Kivelson, *Nature*, **347**, 434 (1995);
- ⁶ F. Pistolesi and G. C. Strinati, *Phys. Rev. B* **53**, 15 168 (1996); N. Andrenacci *et al.*, *Phys. Rev. B* **60**, 12410 (1999).
- ⁷ S.H. Pan *et al.* *Nature (London)*, **413**, 282 (2001).
- ⁸ I. Iguchi, T. Yamaguchi, and A. Sugimoto, *Nature (London)*, **412**, 420 (2001).
- ⁹ See, e.g., C. P. Poole, H. A. Farach, and R. J. Creswick, *Superconductivity* (Academic Press, New York, 1995).
- ¹⁰ Y.J. Uemura *et al.*, *Phys. Rev. Lett.* **62**, 2317 (1989).
- ¹¹ A. Moreo, D.J. Scalapino, and S.R. White, *Phys. Rev. B* **45**, 7544(R) (1992).
- ¹² J. M. Singer, M.H. Pedersen, T. Schneider, H. Beck and H.-G. Matuttis, *Phys. Rev. B*, **54**, 1286 (1996).
- ¹³ J. M. Singer, T. Schneider, M.H. Pedersen, *Eur. Phys. J. B* **2**, 17 (1998).
- ¹⁴ S. Moukouri, Y. M. Vilks, and A.-M. S. Tremblay *Phys. Rev. Lett.* **83**, 4128 (1999).
- ¹⁵ A. Sewer, X. Zotos and H. Beck, *Phys. Rev. B*, **66**, 140504R (2002).
- ¹⁶ A. Georges, G. Kotliar, W. Krauth, and M. J. Rozenberg, *Rev. Mod. Phys.* **68**, 13 (1996).
- ¹⁷ Y.M. Vilks and A.-M.S. Tremblay, *J. Phys. I France* **7**, 1309 (1997); B. Kyung, S. Allen, and A.-M. S. Tremblay, *Phys. Rev. B* **64**, 075116 (2001).
- ¹⁸ See, for example, A. Auerbach, *Interacting Electrons and Quantum Magnetism*, Springer-Verlag, New York, 1994.
- ¹⁹ M. Keller, W. Metzner, and U. Schollwöck, *Phys. Rev. Lett.* **86**, 4612 (2001).
- ²⁰ M. Capone, C. Castellani, and M. Grilli, *Phys. Rev. Lett.* **88**, 126403 (2002).
- ²¹ M. Caffarel and W. Krauth, *Phys. Rev. Lett.* **72**, 1545 (1994).
- ²² G. Kotliar, E. Lange, and M. J. Rozenberg *Phys. Rev. Lett.* **84**, 5180 (2000).
- ²³ G. Moeller, Q. Si, G. Kotliar, M.J. Rozenberg, and D. S. Fisher, *Phys. Rev. Lett* **74**, 2082 (1995).
- ²⁴ G. Kotliar, *Eur. Phys. Jour. B* **11** 27 (1999).
- ²⁵ M. Keller, W. Metzner, and U. Schollwöck, *J. Low Temp. Phys.* **126**, 961 (2002).
- ²⁶ H. Heiselberg, C. J. Pethick, H. Smith, and L. Viverit, *Phys. Rev. Lett.* **85** 2418 (2002).
- ²⁷ See, e.g., A. Perali, P. Pieri, G.C. Strinati, and C. Castellani, *Phys. Rev. B*, **66**, 024510 (2002).
- ²⁸ M. Capone, M. Fabrizio, C. Castellani, and E. Tosatti, *Science*, **296**, 2364 (2002).
- ²⁹ M. Capone, M. Fabrizio, C. Castellani, and E. Tosatti, *Phys. Rev. Lett* **93**, 047001 (2004)